RESEARCH PAPER

# Influence of Annealing Temperature on Structural and Electrical Properties of Screen Printed Lanthanum Oxide Thick Films

**Sonali Laxman Wagh[1,*], Umesh Jagannath Tupe[2], Anil Bhimrao Patil[1], Arun Vitthal Patil[3]**

* *sonalilwagh@gmail.com*

[1] Department of Electronic Science and Research Center, Loknete Vyankatrao Hiray Arts, Science and Commerce College, Panchavati, Nashik, Affiliated to SPPU, Pune, Maharashtra, 422003, India
[2] Department of Electronics, Vidya-Amrut Dnyan Pratishtan's, Arts, Science & Commerce College, Shirsondi, Affiliated to SPPU, Pune, Tal: - Malegaon Dist: - Nashik, Affiliated to SPPU, Maharashtra– 423208, India
[3] Department of Physics, MGV's, Arts, Science and Commerce College, Manmad, Dist. Nashik, Affiliated to SPPU, Pune, Maharashtra - 423104, India

**Received: June 2022** **Revised: November 2022** **Accepted: December 2022**
***DOI: 10.22068/ijmse.2716***

***Abstract:*** *Temperature is one of the key factor that affecting the electrical, physical, structural, and morphological properties as well as the crystallinity of the nanomaterials. The current study investigates the effect of annealing temperature on the structural and electrical properties of lanthanum oxide ($La_2O_3$) thick films. $La_2O_3$ thick films were prepared on a glass substrate using a conventional screen printing technique. In this work, T1 is an unannealed prepared film, whereas T2 and T3 are annealed in a muffle furnace for 3 hours at 350°C and 450°C, respectively. XRD technique was exploited to investigate the crystallization behavior of the films. It was found that the crystal structure of $La_2O_3$ thick films are pure hexagonal phase. The annealing temperatures were revealed to have influence on the crystallite sizes of the films. SEM and EDS was used to study the morphology and elemental analysis of the films respectively. The electrical properties of the films were explored by measuring resistivity, temperature coefficient of resistivity (TCR), and activation energy at lower and higher temperatures regions. The film annealed at 450°C has high resistivity, a high TCR, and small crystallite size. The thickness of the $La_2O_3$ thick films was also found to decrease as the annealing temperature increased.*

***Keywords:*** *Lanthanum oxide, annealed, glass substrate, activation energy, structural, electrical properties.*

***Graphical Abstract:***

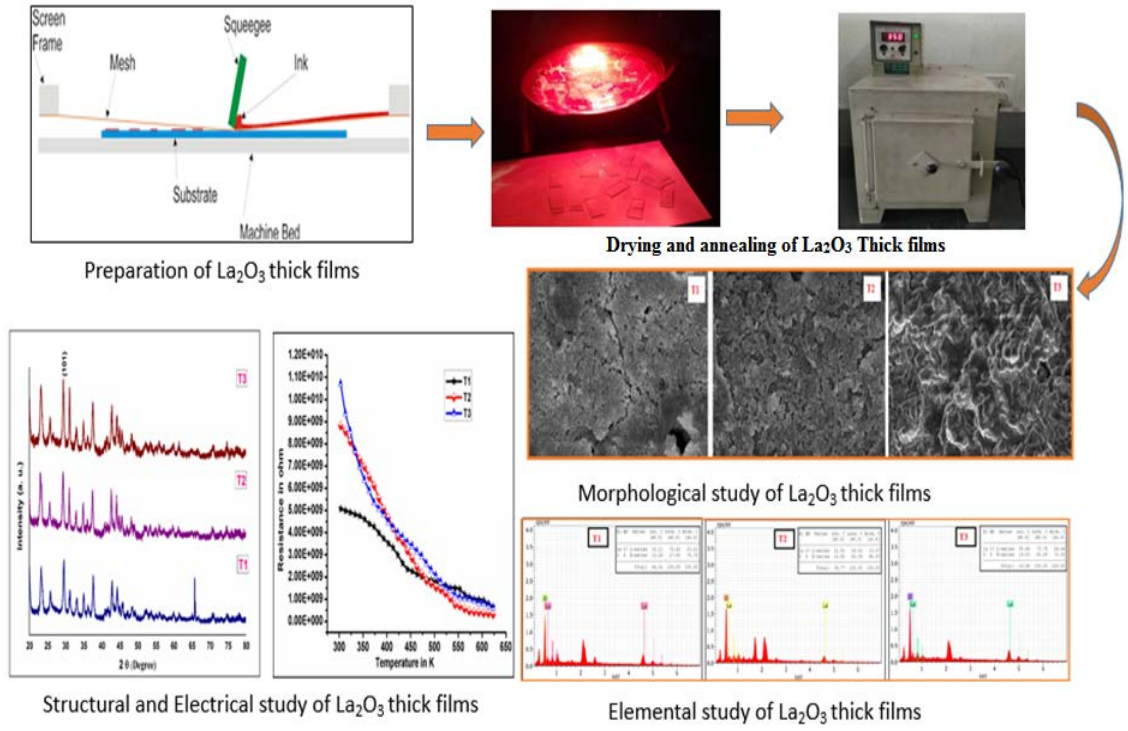

## 1. INTRODUCTION

Lanthanum oxide ($La_2O_3$) is one of the most promising material in advanced metal-oxide semiconductor technology. $La_2O_3$ is an appealing functional rare earth oxide compound that has increasingly piqued the interest of researchers in recent years [1, 2]. Recent research has revealed that $La_2O_3$, as a p-type semiconductor oxide, has unique chemical, thermodynamic, physical, electrical and chemical properties, making it a suitable candidate for use in many areas. By combining the valences $La_3^+/La_2^+$, $La_2O_3$ can use to store energy [3, 4].

$La_2O_3$ is a colourless, odourless substance. It is not soluble in water, although it is soluble in dilute acid. Lanthanum oxide nanoparticles have very high photoelectric conversion efficiency. $La_2O_3$ is a low-cost basic material with a wide spectrum of organic reactions. $La_2O_3$ is a non-toxic substance that is used in a wide range of applications such as gas sensors, catalysts, supercapacitors, batteries, optoelectronics, luminescence, and biomedicine [5, 6].

various variety of approaches were used to synthesis of $La_2O_3$ nanoparticles like sol-gel, spray pyrolysis, solvothermal, thermal decomposition, precipitation, co-precipitation, hydrothermal, Chemical Bath Deposition, Reflux method, Solution combustion, microemulsion method, chemical vapour deposition, sputtering, thermal oxidation, and combustion methods. High crystallisation degree, pure phase, and variable particle size of nano powders or nanoparticles can be obtained using these approaches [6-9].

Annealing is a typical technique for improving thin film adhesion and performance, with its benefits attributed to changes in the nature of the interface and segregant diffusion. By modifying yield qualities, it also impacts plasticity in the process zone [10]. Annealing is the process of atoms or charges restructuring in a material throughout time after irradiation. Although high temperatures may be required to achieve these results, some annealing effects can be achieved at ambient temperature over extended periods of time [11].

Sen B. et. al (2007) reported effect of annealing temperature on thin films using sol gel method. The cell dimensions and unit cell volume continued to shrink as the annealing temperature increased. Furthermore, as the annealing temperatures were raised, the difference between the unit cells of films was found to decrease. This could be owing to a strong ionic interaction between the unit cell's sub-lattice ions when the oxygen stoichiometry and/or oxygen concentration increase with higher annealing temperatures. Increasing the annealing temperature also increases film density and decreases lattice and volume defects, reducing internal stress in the film and reducing cell dimensions [12, 13].

In the field of gas sensor the electrical parameters like resistivity, temperature coefficient of resistivity (TCR), and activation energy are very important. The gas response of the films are depends on these parameters. As well as the structural parameters including morphological, specific surface area, grain size, crystallite size, dislocation density and crystallinity of the nanomaterials also plays a vital role for gas sensing mechanism. Hence the current research work focus on the study of influence or impact of annealing temperature on the structural and electrical properties of $La_2O_3$ thick films prepared by conventional screen printing technique.

## 2. EXPERIMENTAL WORK

### 2.1. Preparation of $La_2O_3$ Thick Films by Standard Screen-Printing Technique

In this experiment work, commercially available AR grade (99.99% purity) Lanthanum oxide nano powder was used. On a clean glass substrate, all $La_2O_3$ films were prepared. All glass substrates were thoroughly cleaned with double distilled water and acetone and exposed to an IR lamp for 30 minutes to remove contaminants. Pure thick films of $La_2O_3$ were prepared using a mixture of 70% inorganic and 30% organic materials. Inorganic materials included commercially available $La_2O_3$ nano powder while organic materials included ethyl cellulose and butyl carbitol acetate (BCA). The $La_2O_3$ powder and ethyl cellulose were combined and mixed together in a mortar and pestle then adding BCA drop by drop to make a thixotropic paste. To prepare thick films, this paste was uniformly applied to a glass substrate through a screen printing technique. The thick films were prepared and exposed to IR radiation for 45-50 minutes to eliminate any residual impurities and local binder.

After that some prepared thick films were annealed at 350°C and 450°C in a muffle furnace for 3 hours and then used future study.
The prepared thick films unannealed and annealed at 350, and 400°C temperatures are labelled as T1, T2 and T3 respectively in all further discussions.

### 2.2. Structural Characterization

The standard tools like XRD, FESEM, and EDS were used to study the structural characteristics, surface morphology, and elemental composition of the prepared $La_2O_3$ thick films, respectively. The mass difference method was used to determine the thickness of the prepared thick films [14]. The prepared films thickness was found to be in the μm range.

#### *2.2.1. X-Ray Diffraction*

XRD patterns of $La_2O_3$ thick films were recorded on Rigaku diffractometer (DMAX-500), X-ray diffractometer with CuKα radiation and wavelength λ= 1.54059 A°. The samples were scanned for 2θ ranges from 10° to 80°. The obtained values of 2θ were compared with Joint Committee on Powder Diffraction Standards (JCPDS) data files. Full width of half maxima was calculated using origin 9 software. The crystallite size (D) was calculated by Debye Scherer's formula [14] that is Eq. 1.
Rigaku diffractometer (DMAX-500), X-ray diffractometer with CuKα radiation and wavelength λ= 1.54059 A°, was used to record XRD patterns of prepared $La_2O_3$ thick films. The films were examined for two different ranges ranging from 10° to 80°. The obtained 2θ values were compared to standard data files from the Joint Committee on Powder Diffraction Standards (JCPDS). Origin 9.5 software was used to compute the full width of half maxima of obtained prominent peak in XRD plot. Debye Scherer's formula, Eq. 1, was used to calculate the crystallite size (D).

$$D = \frac{K\lambda}{\beta \cos\theta} \quad (1)$$

Where, K= Scherrer constant (0.9), β= Full width of half maxima (FWHM),
λ =wavelength of X source (1.540598 A°)

#### *2.2.2. FESEM and EDAX*

The surface morphology of the prepared thick films was characterized using Field Emission Scanning Electron Microscopy (FESEM) [Model JOEL 6300 LA GERMANY]. Using Image-J software, the spherical size particle diameter of $La_2O_3$ thick film was calculated. An energy dispersive X-ray spectrometer (EDAX) [JOEL-2300, Germany] was used to conduct the elemental composition of prepared films. FESEM images and the Brunauer-Emmett-Teller (BET) method were used to calculate the surface area of unannealed and annealed films [14].

### 2.3. Electrical Characterization

The half bridge method was used to determine the DC resistance of the films as a function of temperature. A constant DC voltage was provided to the circuit and the thick film was connected in series with an external load resistor RL. The output voltage across the RL resistor was measured with a digital multimeter (classic 5175 DM, 0.5) to determine the film resistance values. A chromel-alumel thermo-couple was used to indicate the operating temperature on a digital temperature display device. Equations 2, 3, and 4 were used to compute the resistivity, temperature coefficient of resistance and activation energy at lower and higher temperature region of the prepared $La_2O_3$ thick films [14, 15].

$$p = \left(\frac{R \times b \times t}{l}\right) \text{ohm} - \text{m} \quad (2)$$

Where,
R= Resistance of the film at room temperature, t= thickness of the film,
b= breadth of the film, *l*= length of the film.

$$\text{TCR} = \frac{1}{R_0}\frac{\Delta R}{\Delta T}/^{\circ}\text{C} \quad (3)$$

Where,
ΔR= change in resistance between temperature $T_1$ and $T_2$,
ΔT= temperature difference between $T_1$ and $T_2$ and
$R_0$= Resistance of the film at room temperature.

$$\Delta E = \frac{\log R}{\log Ro} \times KT \quad (4)$$

Where,
ΔE= Activation energy, R= Resistance at elevated temperature, $R_0$= Resistance at 0°C.

## 3. RESULT AND DISCUSSION

### 3.1. Structural properties

#### *3.1.1. X-Ray Diffraction (XRD)*

The XRD analysis was performed to determine the crystal structure of the prepared thick films. The X-ray diffraction patterns of $La_2O_3$ are depicted in Fig. 1. T1 is an unannealed prepared film, whereas T2 and T3 indicate annealed

prepared films at 350°C and 450°C, respectively. The overall crystal structure of $La_2O_3$ thick films is revealed by XRD patterns. By using 2θ value the prominent peak was found at 29.58°, 29.34° and 29.44° to T1, T2 and T3 samples respectively as shown in Fig. 1. The crystal structure was found to be pure hexagonal phase for lanthanum oxide and the diffraction peak observed at (101) reflection plane. These results were match with standard JCPDS card No. 83-1348 [7]. The strong, and sharp diffraction peaks confirmed crystallinity of $La_2O_3$. The nanostructures of $La_2O_3$ are indicated by the broader nature of the XRD peaks. From the XRD pattern of T2 and T3 it is found the height and the FWHM value of prominent peak is decreased and decreased respectively as shown in table 1. As compare to JCPDS card No. 83-1348 the prominent peaks are shifted due to annealing.

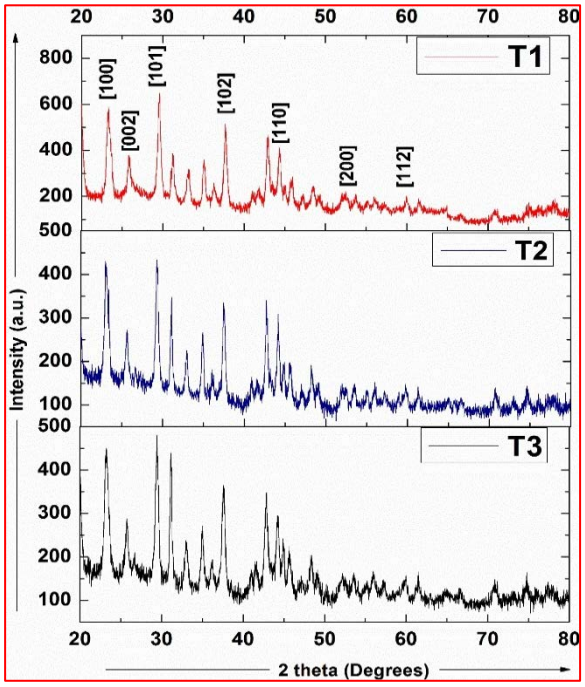


**Fig. 1.** XRD pattern of unannealed $La_2O_3$ thick films (T1), XRD pattern of $La_2O_3$ thick films annealed at 350°C (T2), XRD pattern of $La_2O_3$ thick films annealed at 450°C (T3)

By using Debye-Scherrer formula equation 1, the crystalline size of T1, T2 and T3 was determined 20.11 nm, 22.53 nm and 19.51 nm respectively. It is also found that the as annealing temperature increases the crystalline size increased for T2 and decreased for T3 samples. The small crystallite size (D) influence the specific surface area of the film. As crystallite size reduces the specific surface area increases, which is important to gas sensing properties of the films.

### *3.1.2. Field Emission Scanning Electron Microscopy (FESEM)*

Surface properties of materials are frequently examined using FESEM magnification at 10K. Surface features such as homogenous, heterogeneous, porosity, and voids can be visualised by SEM investigation of the materials [14].

FESEM micrographs of unannealed and annealed $La_2O_3$ thick films are shown in Fig. 2. Field emission scanning electron microscopy was used to characterize the microstructure. The samples T1 and T2 shows microstructure is fairly homogeneous, with small open porosity, according to FESEM micrographs. There was, nevertheless, considerable residual intragranular porosity to sample T1. It was observed that as the annealing temperature was raised, the grain size and crystalline quality changes. The atoms can be shifted to more energetically favorable places such as voids, grain boundaries, and interstitial locations as a result of annealing. As the temperature rises, the crystallinity improves, increasing the mobility of atoms at the of films surface [15, 16]. The sample T3 shows good adhesion and more porosity as compare to T1 and T2 samples, it may be the annealing temperature of sample T3 is more as compare to T1 and T2 samples.

### *3.1.3. Energy Dispersive X-ray Spectrometer (EDAX)*

The elemental composition of the films unannealed and annealed at 350°C and 450°C is shown in Table 2. From Fig. 3, both lanthanum and oxygen peaks can be seen in the EDAX spectra, with no impurities in all samples.

**Table 1.** XRD parameters of $La_2O_3$ thick films

| Sample | 2 Theta (Degree) | FWHM | Max. Intensity (A.U) | Crystallite Size (nm) |
|---|---|---|---|---|
| T1 | 29.58 | 0.427 | 648 | 20.11 |
| T2 | 29.34 | 0.381 | 434 | 22.53 |
| T3 | 29.44 | 0.440 | 480 | 19.51 |

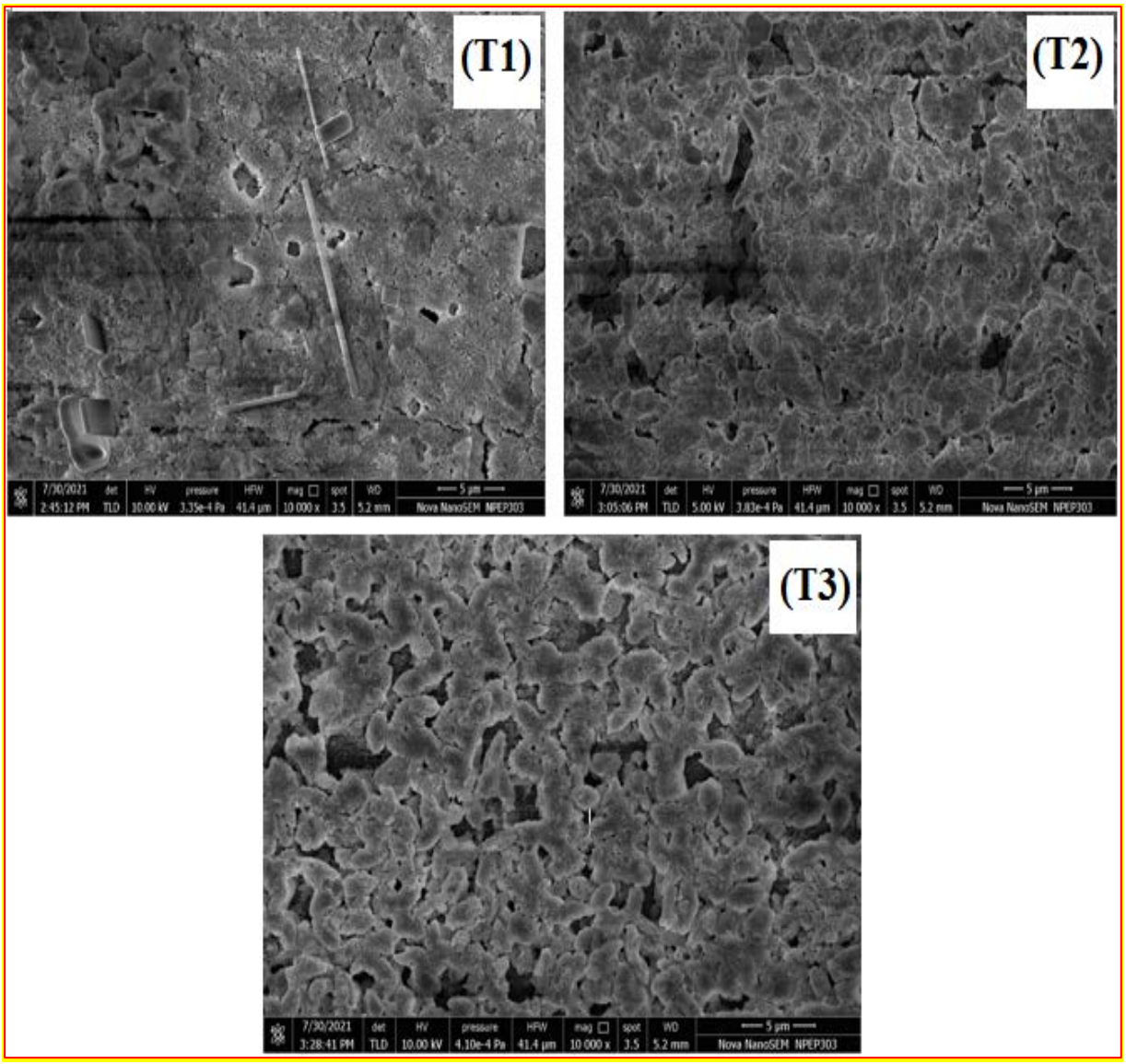


**Fig. 2.** FESEM micrographs of unannealed $La_2O_3$ thick films (T1), FESEM micrographs of $La_2O_3$ thick films annealed at 350°C (T2), FESEM micrographs of $La_2O_3$ thick films annealed at 450°C (T3)

Due to the release of extra oxygen, the mass percentage of oxygen in the T3 sample decreased as the annealing temperature was increased. According to the results, $La_2O_3$ thick films are non-stoichiometric [15, 17].

## 4. ELECTRICAL PROPERTIES

### 4.1. Resistivity

Fig. 4 depicts the resistance of prepared $La_2O_3$ thick films samples in air as a function of temperature for T1, T2 and T3 samples. Resistance decreases as temperature rises, showing semiconducting behaviour.

Any increase in the temperature of a thick film leads electrons to gain enough energy to overcome the grain boundary barrier. Because oxygen adsorbates are desorbed from the surface of the films at higher temperatures, the potential barrier at grain boundries may be reduced. The carrier concentration rises at higher temperatures due to intrinsic thermal excitation, and the electron transport process enhances as the temperature rises.

The thick film's resistance decreases as temperature rises, which could be owing to increased charge carrier drift mobility or increased lattice vibrations, in which the atoms periodically come close enough for charge carrier transfer and conduction is generated by lattice vibration [15-18].

**Table 2.** Composition of $La_2O_3$ thick films

| Sample | Element | At. Wt. % | Mass % |
|---|---|---|---|
| T1 | La<br>O | 23.21<br>76.79 | 72.40<br>27.60 |
| T2 | La<br>O | 13.07<br>86.93 | 56.62<br>43.38 |
| T3 | La<br>O | 24.44<br>75.56 | 73.74<br>26.26 |

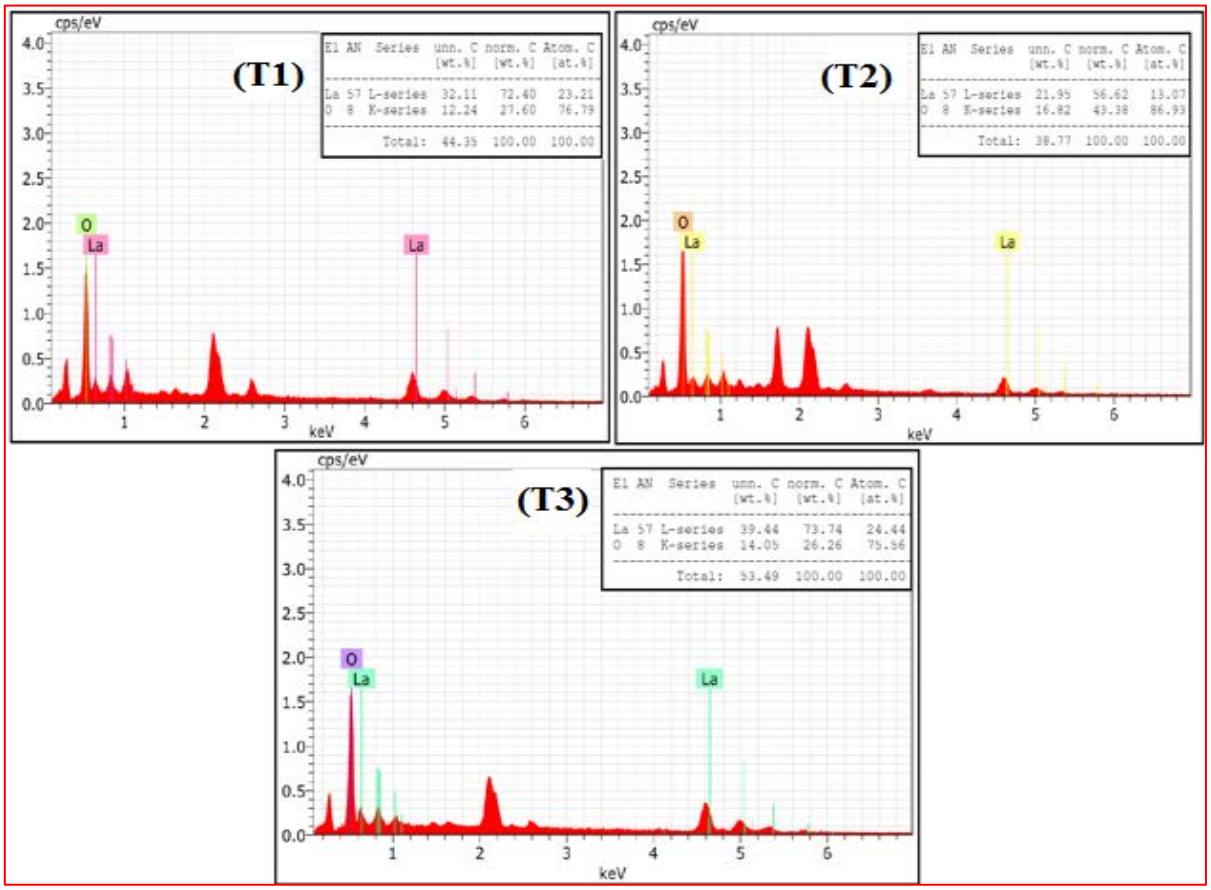


**Fig. 3.** EDAX spectrum of unannealed $La_2O_3$ thick films (T1), EDAX spectrum of $_{La2O3}$ thick films annealed at 350 °C (T2), EDAX spectrum of $La_2O_3$ thick films annealed at 450 °C (T3).

From Fig. 4, it is also observed that the resistance of prepared $La_2O_3$ thick films samples reduces rapidly from ambient temperature to a particular temperature range, whereas the resistance drops slowly at higher temperatures. Due to the graph's exponential structure, the resistance attain a constant lowest saturation level with respect to temperature. Equation 2 is used to calculate the resistivity of prepared $La_2O_3$ thick film samples at constant temperature. The resistivity of T1, T2 and T3 samples was found to be 65971.69 Ω-m, 96948.83 Ω-m and 1101690.72 Ω-m respectively. It is also found that the as annealing temperature increases the resistivity of prepared $La_2O_3$ thick film samples increased. The gas sensors constructed using metal oxide semiconductors (MOS) in which resistance as well as resistivity is a key parameter because the sensing behaviour/principle of MOS sensor depends on the change in resistance with nature of gas (oxidizing or reducing).

#### *4.1.1. Temperature Coefficient of Resistance (TCR)*

The influence of temperature on resistance was examined in order to compute the TCR, which was calculated using Equation 3. TCR of prepared $La_2O_3$ thick film was negative for all samples, indicating that the thick films were

semiconducting nature. The variation of TCR with prepared $La_2O_3$ thick film samples is shown in Fig. 5. TCR is found to be negative, and its value dropped to T2 sample and raised to T3 sample as the annealing temperature was increased. TCR increased gradually with increasing annealing temperature in the T3 sample, indicating an electron emission mechanism that expanded exponentially with increasing annealing temperature [15, 20]. The TCR of T1, T2 and T3 samples was found to be -0.0049678/°C, -0.0054271/°C and -0.0036719/°C respectively.

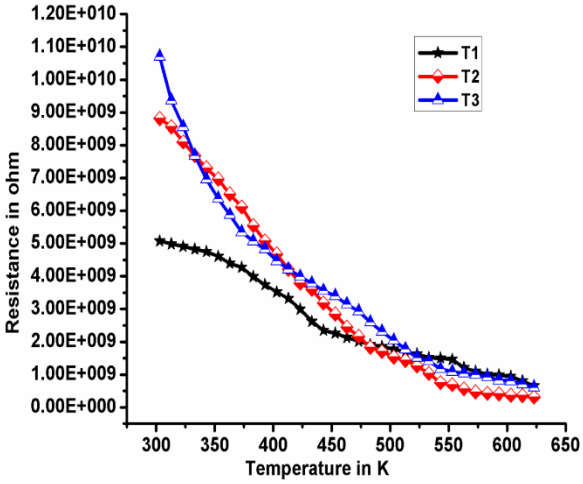


**Fig. 4.** Resistance v/s temperature graph of unannealed $La_2O_3$ thick films (T1), Resistance v/s temperature graph of La2O3 thick films annealed at 350°C (T2), Resistance v/s temperature graph of La2O3 thick films annealed at 450°C (T3)

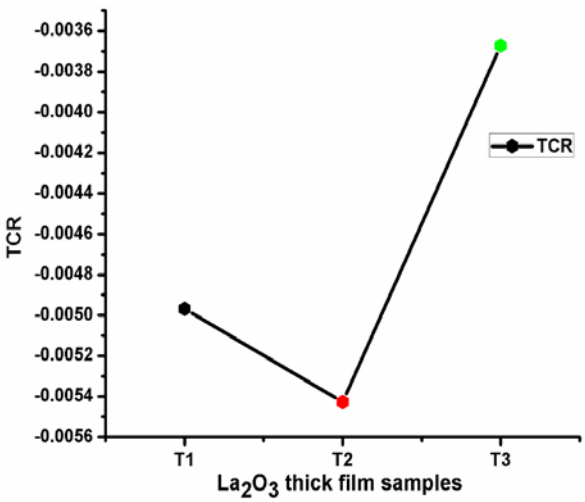


**Fig. 5.** TCR of unannealed $La_2O_3$ thick films (T1), TCR of $La_2O_3$ thick films annealed at 350°C (T2), TCR of $La_2O_3$ thick films annealed at 450°C (T3)

### *4.1.2. Activation Energy*

The Arrhenius plot of Log Rs v/s 1/T for prepared $La_2O_3$ thick film samples is shown in Fig. 6. Because material passes from one conduction mechanism to another, the activation energy in the low temperature region is always lower than the energy in the high temperature region. The rise in conductivity in the low-temperature region is due to the mobility of charge carriers, which is dependent on the defects concentration. As a result, the region of low temperature conduction is commonly referred to as the conduction mechanism. Because low thermal energies are adequate for the activation of charge carriers to participate in the conduction process, activation energy reduces in this range. In other words, imperfections in the lattice that are loosely attached can simply transfer. As a result, an increase in conductivity at lower temperatures can be attributed to a rise in charge mobility.

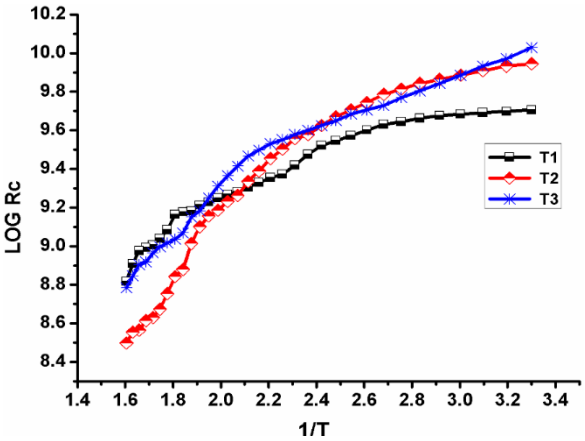


**Fig. 6.** Log Rc Vs 1/T of unannealed $La_2O_3$ thick films (T1), Log Rc Vs 1/T of La2O3 thick films annealed at 350°C (T2), Log Rc Vs 1/T of $La_2O_3$ thick films annealed at 450°C (T3)

The activation energy in a high-temperature region is larger than in a low-temperature region [15, 16]. The electrical conductivity in this region is mostly determined by intrinsic imperfections; hence it is referred to as intrinsic conduction. The high activation energy values in this region can be driven by the fact that the energy necessary to generate the imperfections is significantly more than that required to drift it. As a result, only at high temperatures the intrinsic imperfections generated by thermal fluctuations impact the electrical conductivity of the films [15, 18, 20]. Equation 4 is used to calculate the action energy

at higher and lower regions of prepared $La_2O_3$ thick film samples. The action energy at higher region of T1, T2 and T3 samples was found to be 0.160346 eV, 0.772415 eV and 0.26699 eV respectively and the action energy at lower region of T1, T2 and T3 samples was found to be 0.00846831 eV, 0.123552 eV and 0.097387 eV respectively.
Table 3 summarizes the influence of annealing on the electrical properties of prepared $La_2O_3$ thick films.

## 5. CONCLUSIONS

$La_2O_3$ thick films could be prepared using screen printing technique on a glass substrate. The crystal structure of $La_2O_3$ thick films was found to be pure hexagonal phase, according to XRD analysis. The voids between the particles were found using FESEM micrographs to be caused by the evaporation of the organic solvent during the annealing of the prepared films. The films annealed at 450°C (sample T3) are found to have a high resistivity, a high TCR, and a small crystallite size. The thickness of the $La_2O_3$ thick films was also found to decrease as the annealing temperature increased. The obtained results are helpful in the field of gas sensor.
The impact of annealing temperature on prepared thick films were studied. According to obtained results few important points were observed those listed are below-
The annealing temperature increased-

1. From XRD, the size of crystallite (D) decreased.
2. The resistivity of the $La_2O_3$ thick films decreased.
3. The TCR of the $La_2O_3$ thick films increased.
4. The thickness of the $La_2O_3$ thick films decreased.
5. From FESEM, the morphology of $La_2O_3$ thick films changes (more porosity/voids was found)

## ACKNOWLEDGMENT

The authors thank to Head, Department of Electronic Science and Research Center, L. V. H. College, Nashik, Maharashtra, India, for providing laboratory facilities.
The authors also acknowledge and pay sincere thanks to Head, Department of Physics, S. P. Pune University, Pune and B. R. Gholap College, Pune, India for providing the laboratory facilities for SEM, EDAX and XRD characterization for present research work.
This research received no specific grant from any funding agency.
The authors have no conflicts of interest to disclose.

## REFERENCES:

[1] Goh KH, Haseeb AS, Wong YH. Lanthanide rare earth oxide thin film as an alternative gate oxide. Materials Science in Semiconductor Processing. 2017 Sep 1; 68:302-15.
[2] Yang C, Fan H, Qiu S, Xi Y, Fu Y. Microstructure and dielectric properties of $La_2O_3$ films prepared by ion beam assistant electron-beam evaporation. Journal of Non-Crystalline Solids. 2009 Jan 1; 355(1):33-7.
[3] Miranda E, Molina J, Kim Y, Iwai H. Tunneling in sub -5 nm $La_2O_3$ films deposited by E-beam evaporation. Journal of non-crystalline solids. 2006 Jan 1; 352(1):92-7.
[4] Yang C, Fan H, Qiu S, Xi Y, Fu Y. Microstructure and dielectric properties of La2O3 films prepared by ion beam assistant electron-beam evaporation. Journal of Non-Crystalline Solids. 2009 Jan 1; 355(1):33-7.
[5] Vignolo MF, Duhalde S, Bormioli M, Quintana G, Cervera M, Tocho J. Structural and electrical properties of lanthanum oxide thin films deposited by laser ablation. Applied surface science. 2002 Sep 30; 197:522-6.
[6] Dabhane, H., Ghotekar, S., Tambade, P. and Medhane, V., 2020. Plant mediated green synthesis of lanthanum oxide (La2O3) nanoparticles: A review. Asian Journal of Nanosciences and Materials, 3(4):291-299.
[7] Kabir H, Nandyala SH, Rahman MM, Kabir MA, Stamboulis A. Influence of calcination on the sol–gel synthesis of lanthanum oxide nanoparticles. Applied Physics A. 2018 Dec; 124(12):1-1.

**Table 3.** Summary of thickness, resistivity, activation energy and TCR of prepared $La_2O_3$ thick films

| Sample | Thickness of film (µm) | Resistivity (Ω-m) | TCR (/°C) | Activation energy (eV) | |
|---|---|---|---|---|---|
| | | | | HTR | LTR |
| T1 | 26 | 65971.69 | -0.0049678 | 0.160346 | 0.084683 |
| T2 | 22 | 96948.83 | -0.0054271 | 0.772415 | 0.123552 |
| T3 | 19 | 1101690.72 | -0.0036719 | 0.266991 | 0.097387 |


[8] Nejad SJ, Abolghasemi H, Moosavian MA, Golzary A, Maragheh MG. Fractional factorial design for the optimization of hydrothermal synthesis of lanthanum oxide nanoparticles under supercritical water condition. The Journal of Supercritical Fluids. 2010 Apr 1; 52(3):292-7.

[9] Sheng J, Zhang S, Lv S, Sun W. Surfactant-assisted synthesis and characterization of lanthanum oxide nanostructures. Journal of materials science. 2007 Dec; 42(23):9565-71.

[10] Koli PB, Kapadnis KH, Deshpande UG, Tupe UJ, Shinde SG, Ingale RS. Fabrication of thin film sensors by spin coating using sol-gel $LaCrO_3$ Perovskite material modified with transition metals for sensing environmental pollutants, greenhouse gases and relative humidity. Environmental Challenges. 2021 Apr 1; 3:100043.

[11] Shinde VS, Kapadnis KH, Sawant CP, Koli PB, Patil RP. Screen print fabricated In3+ decorated perovskite lanthanum chromium oxide ($LaCrO_3$) thick film sensors for selective detection of volatile petrol vapors. Journal of Inorganic and Organometallic Polymers and Materials. 2020 Dec; 30 (12):5118-32.

[12] Sen B, Wong H, Molina J, Iwai H, Ng JA, Kakushima K, Sarkar CK. Trapping characteristics of lanthanum oxide gate dielectric film explored from temperature dependent current–voltage and capacitance–voltage measurements. Solid-state electronics. 2007 Mar 1; 51 (3):475-80.

[13] Salinas, D., Sepúlveda, C., Escalona, N., Gfierro, J.L. and Pecchi, G., 2018. Sol–gel $La_2O_3$–$ZrO_2$ mixed oxide catalysts for biodiesel production. Journal of energy chemistry, 27(2): 565-572.

[14] Singh RD, Koli PB, Jagdale BS, Patil AV. Effect of firing temperature on structural and electrical parameters of synthesized $CeO_2$ thick films. SN Applied Sciences. 2019 Apr; 1 (4):1-9.

[15] Adole VA, Pawar TB, Koli PB, Jagdale BS. Exploration of catalytic performance of nano-$La_2O_3$ as an efficient catalyst for dihydropyrimidinone/thione synthesis and gas sensing. Journal of Nanostructure in Chemistry. 2019 Mar; 9(1):61-76.

[16] Dighavkar CG, Patil AV, Patil SJ, Borse RY. Influence of Firing Temperature on Compositional and Structural Properties of $TiO_2$ Thick Films. Invertis Journal of Science & Technology. 2010; 3 (3):184-93.

[17] Mangla O, Srivastava A, Malhotra Y, Ostrikov K. Lanthanum oxide nanostructured films synthesized using hot dense and extremely non-equilibrium plasma for nanoelectronic device applications. Journal of Materials Science. 2014 Feb; 49(4):1594-605.

[18] Koli PB, Kapadnis KH, Deshpande UG, Tupe UJ, Shinde SG, Ingale RS. Fabrication of thin film sensors by spin coating using sol-gel $LaCrO_3$ Perovskite material modified with transition metals for sensing environmental pollutants, greenhouse gases and relative humidity. Environmental Challenges. 2021 Apr 1; 3:100043.

[19] Yang Z, Kumar A. The impacts of thermal pretreatments on biomass gasification and pyrolysis processes. InBiomass Preprocessing and Pretreatments for Production of Biofuels 2018 Jul 26 (pp. 292-324). CRC Press.

[20] Tupe UJ, Zambare MS, Patil AV, Koli PB. The Binary Oxide NiO-CuO Nanocomposite Based Thick Film Sensor for the Acute Detection of Hydrogen Sulphide Gas Vapours. Material Science Research India. 2020; 17(3):260-9.